

# Hydrogen activation over stoichiometric and defective CeO<sub>2</sub> surfaces: A first-principles study

Chen Zihui<sup>1</sup>, Zhao Chuanlin<sup>1</sup>, Liu Jinxun<sup>1\*</sup>, Li Weixue<sup>1,2\*</sup>

1. Department of Chemical Physics, School of Chemistry and Materials Science, University of Science and Technology of China, Hefei 230026, China;  
2. Hefei National Laboratory for Physical Sciences at the Microscale, University of Science and Technology of China, Hefei 230026, China  
\* Corresponding author. E-mail: jxliu86@ustc.edu.cn; wxli70@ustc.edu.cn

**Abstract:** Hydrogen activation plays a pivotal role in hydrogenation reactions over transition metal oxide catalysts. Clarifying hydrogen activation over ceria oxide (CeO<sub>2</sub>) is an important issue in the acetylene hydrogenation reaction. Employing density functional theory (DFT) calculations, we studied hydrogen activation over stoichiometric and defective CeO<sub>2</sub> (111), (110), and (100) surfaces. Hydrogen dissociates on the stoichiometric CeO<sub>2</sub> surfaces only forming hydroxyl groups. The presence of oxygen vacancies can promote the H<sub>2</sub> activation over the defective CeO<sub>2</sub> surfaces. Both H<sup>+</sup> and H<sup>-</sup> species can be found on the defective CeO<sub>2</sub>(111) and (100) surfaces, whereas only H<sup>+</sup> species can be observed on the defective CeO<sub>2</sub>(110) surface. The structure sensitivity of the H<sub>2</sub> activation over the stoichiometric and defective CeO<sub>2</sub> surfaces is correlated with H<sup>+</sup> and H<sup>-</sup> adsorption energies determined by the ability of the surface oxygen vacancy formation and charge distributions of Ce and O ions. Our work provides more insight into H<sub>2</sub> activation on CeO<sub>2</sub>-based catalysts which will guide better catalyst design for hydrogenation reactions.

**Keywords:** CeO<sub>2</sub>; hydrogen activation; surface sensitivity; density functional theory

**CLC number:** O647.1    **Document code:** A

## 1 Introduction

Partial hydrogenation of alkynes to olefins is one of the most important industrial reactions and is widely used to purify olefin streams usually containing acetylenic<sup>[1]</sup>. One of the most commonly used catalysts in partial hydrogenation of alkynes to olefins is Pd which, however, shows a high tendency in excessive hydrogenation in the formation of alkanes and polymerization of alkynes. To tackle this issue, Pd metal alloying with other metals was synthesized to suppress the over-hydrogenation of alkynes<sup>[2-4]</sup>. For example, alloying Pd with a less active metal can weaken acetylene adsorption and destroy the formation of the  $\beta$ -hydride phase thus improving the selectivity of the partial hydrogenation reaction of alkynes toward olefins<sup>[3]</sup>. However, the high cost of Pd limits its scale-up application in the industry. To maximize the atom-utilization efficiency, a variety of single-atom catalysts have been synthesized to catalyze alkynes hydrogenation reaction<sup>[5]</sup>. Many works reported that Pt, Pd, Rh, and other transition metal single atoms deposited on

graphene and black phosphorus show high catalytic activity in alkyne hydrogenation<sup>[6-8]</sup>. However, the single-atom catalysts are often difficult to prepare and ready to aggregate to form large nanoparticles in practice<sup>[5]</sup>. Therefore, it is highly desirable to design catalysts with high stability, activity, and selectivity for alkyne hydrogenation to replace the usage of expensive noble metal catalysts.

As a popular catalytic material, ceria oxide (CeO<sub>2</sub>) is widely used as the support and catalyst<sup>[9-12]</sup> and applied to solid oxide fuel cells<sup>[13,14]</sup> and oxygen sensors<sup>[15,16]</sup>, which is attributed to its low price<sup>[17]</sup>, excellent acid-base properties, and redox properties<sup>[18]</sup>. Consequently, CeO<sub>2</sub> has gained much current interest in catalysis originating from its superior activity and selectivity for many chemical reactions including alkyne semi-hydrogenation reactions<sup>[19-23]</sup>. Pérez-Ramírez and coworkers<sup>[19]</sup> found the conversion of propyne and the selectivity of olefins can be achieved as high as 91% and 96% for propyne hydrogenation reaction over bulk CeO<sub>2</sub> catalyst at the reaction condition of  $T = 523$  K and  $P = 1$  bar with H<sub>2</sub>/C<sub>2</sub>H<sub>2</sub> ratio of 30:1,

respectively. Generally,  $\text{CeO}_2$  displays better catalytic performance in acetylene hydrogenation as compared with conventional noble Pd-based catalysts<sup>[2,24]</sup>. Carrasco and coworkers<sup>[20]</sup> revealed that the hydrogen dissociation has the highest activation barrier and can be considered as the rate-determining step for acetylene hydrogenation over the  $\text{CeO}_2(111)$  surface. Consistent with this work, many groups<sup>[25,26]</sup> also demonstrated the difficulty of hydrogen activation in the hydrogenation of alkynes over the  $\text{CeO}_2(111)$  surface or bulks. Since  $\text{H}_2$  activation plays an important role in the acetylene and/or alkynes hydrogenation reaction, the exploration of  $\text{H}_2$  activation over the  $\text{CeO}_2$  surfaces is pivotal to design better  $\text{CeO}_2$ -based catalysts for acetylene and/or alkynes hydrogenation.

Different from metals, there are generally two different routes for the  $\text{H}_2$  dissociation over metal oxide surfaces, namely, homolytic and heterolytic dissociation of  $\text{H}_2$ . The homolytic  $\text{H}_2$  dissociation often generates two OH groups over metal oxides that are difficult to be reduced, such as  $\text{MgO}$ <sup>[27,28]</sup>,  $\text{Al}_2\text{O}_3$  and  $\text{SiO}_2$ <sup>[29]</sup>. Whereas heterolytic  $\text{H}_2$  dissociation generates an H cation bound to O anion and an H anion bound to the metal cation. Many experimental and theoretical works indicate that the heterolytic  $\text{H}_2$  dissociation is more likely to occur over reducible oxides<sup>[30–32]</sup>, such as  $\text{CeO}_2$ <sup>[33]</sup> and  $\text{TiO}_2$ <sup>[34]</sup>. Density functional theory (DFT) calculations reported that the homolytic  $\text{H}_2$  dissociation is dominant on  $\text{CeO}_2(111)$ <sup>[20,30]</sup> with an activation barrier larger than 1 eV. Therefore, the  $\text{H}_2$  dissociation is difficult on the  $\text{CeO}_2(111)$  surface at a relatively low temperature corroborated by the experimental measurements<sup>[19,20]</sup>. A similar high activation barrier of the  $\text{H}_2$  dissociation was also found for the reverse methanol-reforming reaction over different kinds of  $\text{CeO}_2$  surfaces<sup>[22]</sup>.

In contrast to a well-defined  $\text{CeO}_2(111)$  surface, the heterolytic  $\text{H}_2$  dissociation is more kinetically feasible over the reduced  $\text{CeO}_2(111)$  surfaces<sup>[1,35,36]</sup>. The presence of surface oxygen vacancies ( $\text{V}_\text{o}$ ) on  $\text{CeO}_2$  surfaces promotes the cleavage of hybrid H–H bonds and increases the catalytic activity of alkyne hydrogenation<sup>[1,35]</sup>. Ramirez-Cuesta et al.<sup>[37]</sup> gave the first direct evidence for the presence of both surfaces and bulk Ce–H species on partially reduced ceria rods via in situ inelastic neutron scattering spectroscopy. A new heterolytic  $\text{H}_2$  dissociation mechanism was proposed by Huang et al.<sup>[36]</sup> that the dissociated H species might be bound to  $\text{Ce}_{\text{V}_\text{o}}^{3+}$  sites in the form of hydrides over the reduced  $\text{CeO}_{2-x}(111)$  thin films and  $\text{CeO}_{2-x}$  powders at room temperature. Therefore, heterolytic  $\text{H}_2$  dissociation forming H anion species binding Ce cation is feasible

over the reduced  $\text{CeO}_2(111)$  surface. Besides the oxygen vacancy effect on the  $\text{H}_2$  activation, many studies demonstrated the reactivities of  $\text{H}_2$  activation and acetylene hydrogenation reactions are often surface orientation dependent on  $\text{CeO}_2$  catalysts<sup>[38–40]</sup>. For example, it was found that  $\text{C}_2\text{H}_2$  hydrogenation reaction prefers to occur on polyhedral  $\text{CeO}_2$  particles, whereas the CO oxidation reaction tends to take place over  $\text{CeO}_2$  nanocubes and nanorods<sup>[39]</sup>. Calatayud and coworkers<sup>[40]</sup> have investigated seven different  $\text{CeO}_2$  terminations displaying distinct activities in the hydrogen activation, which indicates the strong structure sensitivity of the  $\text{H}_2$  activation over  $\text{CeO}_2$ -based catalysts.

Although many investigations are done, there are still open on whether and why the oxygen vacancy can promote hydrogenation activation over  $\text{CeO}_2$  catalyst and how the different stoichiometric and defective surfaces of  $\text{CeO}_2$  impact  $\text{H}_2$  activation. In the present work, we studied  $\text{H}_2$  activation over the stoichiometric and defective (111), (110), and (100) facets of  $\text{CeO}_2$ . The structure sensitivity of the  $\text{H}_2$  activation and oxygen vacancy effect on  $\text{H}_2$  activation are revealed on  $\text{CeO}_2$ . The most probable H species on the stoichiometric and defective  $\text{CeO}_2$  surfaces are identified. Our work provides more insight into the  $\text{H}_2$  activation over the  $\text{CeO}_2$  based catalyst which guides a better  $\text{CeO}_2$ -based catalyst design for acetylene hydrogenation reactions.

## 2 Computational methods

Spin-polarized periodic density functional theory (DFT) calculations were performed by using the Vienna ab initio simulation package (VASP)<sup>[41,42]</sup>. The exchange-correlation potential was treated by the generalized gradient approximation (GGA) in the Perdew-Burke-Ernzerh (PBE) functional form<sup>[43]</sup>. The projected-augmented wave (PAW) pseudopotentials were utilized to describe the core electrons<sup>[44]</sup>, and the Kohn-Sham valence states were expanded in a plane-wave basis set with the kinetic energy of 400 eV. The Brillouin zone integration was sampled with  $12 \times 12 \times 12$  Monkhorst-Pack mesh k-points for the bulk  $\text{CeO}_2$  calculations. The equilibrium lattice constant for bulk  $\text{CeO}_2$  was optimized to be 5.45 Å, in good agreement with the experimental measurement of 5.41 Å<sup>[45]</sup>. The DFT +  $U$  methodology was used to treat the on-site Coulomb and the exchange interaction of the strongly localized Ce 4f electrons with an effective  $U_{\text{eff}} = 5$  eV. Here, we adopted  $U$  values of 2 eV and 5 eV, which represent a low  $U$  value and a high  $U$  value respectively, to calculate hydrogen dissociation energies on defective  $\text{CeO}_2(111)$  surfaces (Table S1). The difference in  $\text{H}_2$  dissociative

adsorption energies by using a low and a high  $U$  values are 0.29 eV and 1.33 eV forming H<sup>+</sup>/H<sup>-</sup> and H<sup>+</sup>/H<sup>+</sup>, respectively. Different  $U$  values will result in significantly different H<sub>2</sub> dissociative adsorption energies. Hydrogen dissociation on the CeO<sub>2-x</sub>(111) surface is more difficult by using a low  $U$  value which conflicts with the experiment results<sup>[1,36,37]</sup> that oxygen vacancy can promote hydrogen activation. However, a high  $U$  value of 5 eV is considered to provide localization of the electrons left upon oxygen removal from CeO<sub>2</sub><sup>[46]</sup>. Therefore, we used the  $U$  value of 5 eV for the surface adsorption and reaction calculations in the present work.

The O-terminated CeO<sub>2</sub>(111) surface with a (2×2) unit cell, a Tasker Type 2 surface<sup>[47]</sup>, was modeled by a four-layers slab with the bottom two layers fixed at their bulk positions (Figure 1(a)). The CeO<sub>2</sub>(110) with a (2×2) unit cell, a Tasker Type 1 surface<sup>[47]</sup>, was modeled by a periodic five-layers slab with the bottom two layers fixed at their bulk positions (Figure 1(b)). Whereas the O-terminated CeO<sub>2</sub>(100) with (3×3) periodicity, a Tasker Type 3 surface<sup>[47]</sup>, was modeled by a periodic seven-layer slab with the bottom two layers fixed at their bulk positions (Figure 1(c)). To eliminate the dipole moment perpendicular to the CeO<sub>2</sub>(100) surface<sup>[23]</sup>, half of the O atoms from the top layer are removed, which has been commonly applied in many previous computational studies<sup>[48,49]</sup>.

A 3×3×1 Monkhorst-Pack mesh k-points were used for calculations of H<sub>2</sub> activations over three different CeO<sub>2</sub> surfaces. All slabs were separated by a 12 Å vacuum. All structures were relaxed until forces on each ion were less than 0.02 eV/Å, and the convergence criterion for energy was 10<sup>-4</sup> eV. Transition structures (TS) for the considered reaction paths were located by using the climbing-image nudged elastic band (CI-NEB) algorithm. The adsorption energy was calculated as  $E_{\text{ads}} = E_{\text{total}} - E_{\text{slab}} - E_{\text{gas}}$ , where  $E_{\text{total}}$ ,  $E_{\text{slab}}$ , and  $E_{\text{gas}}$  refer to the energy of the slab with adsorbate, the energy of clean CeO<sub>2</sub> surfaces, and the energy of a gas-phase molecule in a neutral state, respectively. The H<sub>2</sub> activation barrier is calculated as the energy difference between the transition state and the adsorption state of H<sub>2</sub> over CeO<sub>2</sub> surfaces.

## 3 Results

### 3.1 Structure sensitivity of H<sub>2</sub> activation over stoichiometric CeO<sub>2</sub> surfaces

We studied H<sub>2</sub> activation over the three low-index facets of CeO<sub>2</sub>(Figure 1), namely (111), (110), and (100) surfaces, which are prototypical examples of three types of ionic crystal facets. The O and Ce atoms are distributed alternately over the O-terminated CeO<sub>2</sub>(111)

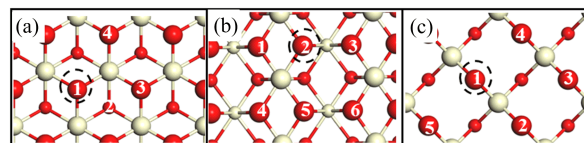


**Figure 1.** The top view of CeO<sub>2</sub>(111) (a), CeO<sub>2</sub>(110) (b) and CeO<sub>2</sub>(100) (c) surfaces. Red and beige spheres are the O and Ce atoms, respectively. Small spheres stand for the subsurface O and Ce atoms. The dashed black circles represent the oxygen vacancies. This notation is used throughout this paper. The indicated numbers are non-equivalent oxygen atoms.

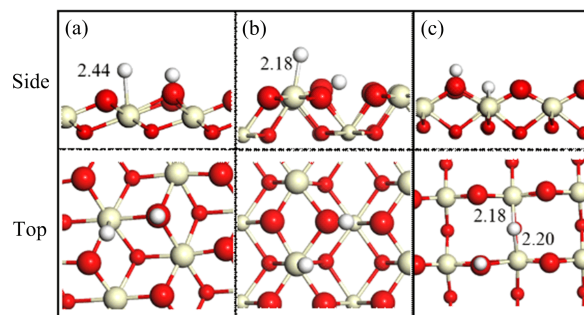


**Figure 2.** Top and side views of optimized configurations for heterolytic H<sub>2</sub> dissociative adsorption over stoichiometric CeO<sub>2</sub>(111) (a), CeO<sub>2</sub>(110) (b), and CeO<sub>2</sub>(100) (c) surfaces. The H-Ce bond distances are indicated in Å.

surface, where the surface O atom is coordinated with three Ce atoms and each Ce atom binds three O atoms. Similarly, O and Ce atoms are distributed alternately on the O-terminated CeO<sub>2</sub>(100) surface, whereas surface O atoms are coordinated with three Ce atoms but each Ce atom binds two surfaces and four lattice oxygen atoms. The O and Ce atoms are distributed in the same layer on the CeO<sub>2</sub>(110) surface, in which the surface O atom binds two Ce atom and Ce atoms are coordinated with four surface and two lattice oxygen atoms. The different surface structures of CeO<sub>2</sub>(111), (110), and (100) surfaces will exhibit the distinct catalytic performance of H<sub>2</sub> activation. H<sub>2</sub> first adsorbs on the CeO<sub>2</sub> surface and then heterolytic dissociate in the formation of an H<sup>+</sup> bound to the O anion and an H<sup>-</sup> bound to the Ce cation (Figure 2). When H atom adsorbs at the O anion site, more electrons can transfer from H to O forming H cation due to the higher electronegativity of O as compared with H. The Bader charges of H atoms at the Ce cation and O anion site are -0.17, -0.15, -0.66 and +0.17, -0.09, +0.21 over CeO<sub>2</sub>(111), (110), and (100) surfaces, respectively (Table S2). Later, the dissociated H atom migrates from the Ce cation to the O anion site. The calculated potential energy surface diagrams and corresponding configurations for H<sub>2</sub> activation are shown in Figure 3.

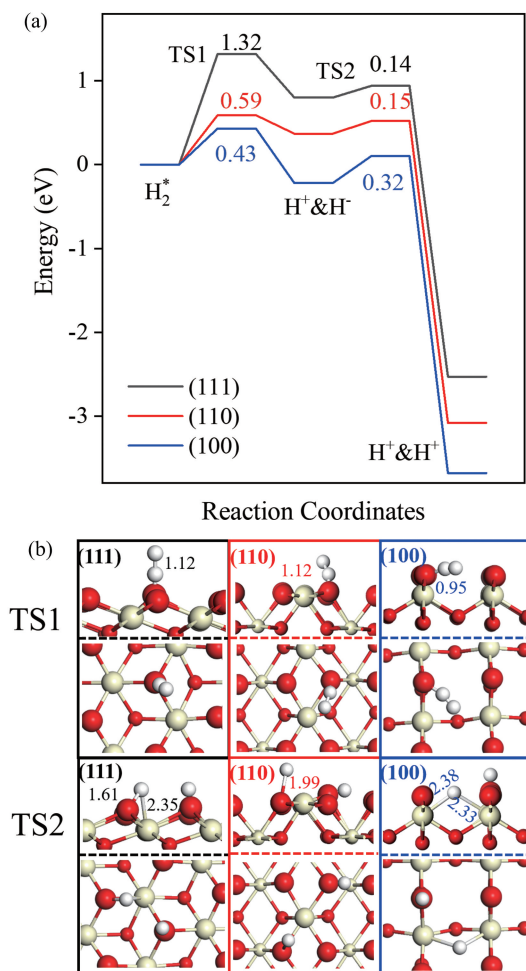


**Figure 3.** The potential energy surface diagram (a) and corresponding transition state configurations (b) for heterolytic H<sub>2</sub> dissociation over the stoichiometric CeO<sub>2</sub>(111), (110), and (100) surfaces. The bond distance between the two dissociated H atoms is indicated in Å.

There is a weak interaction between the H<sub>2</sub> and stoichiometric CeO<sub>2</sub> surfaces and H<sub>2</sub> physically adsorbs on the stoichiometric CeO<sub>2</sub> surfaces with the adsorption energies higher than -0.10 eV. Two different H<sub>2</sub> dissociation mechanisms, namely the heterolytic and homolytic dissociation of H<sub>2</sub>, are considered in the present work. The bond distance of two surface neighboring oxygen atoms in CeO<sub>2</sub> surfaces is larger than 3.85 Å, which is longer than that of the Ce-O bond, the heterolytic H<sub>2</sub> dissociation has a high priority to occur. The limiting distance for homolytic H<sub>2</sub> dissociation to occur is determined by the distance between neighboring surface O atoms. Therefore, we studied the heterolytic dissociation of H<sub>2</sub> at the Ce-O pair (Figure 2), and then the adsorbed H<sup>+</sup> at the Ce cation site might migrate to the O anion thus forming the homolytic H<sub>2</sub> dissociative adsorption modes on CeO<sub>2</sub> surfaces.

The heterolytic dissociation of H<sub>2</sub> is sensitive to the surface structure of CeO<sub>2</sub> from both thermodynamic and kinetic aspects. Specifically, the heterolytic dissociation of H<sub>2</sub> to generate an H<sup>+</sup> and an H<sup>-</sup> is endothermic by 0.80 eV with an activation barrier of 1.32 eV over the CeO<sub>2</sub>(111) surface. The high energy cost and activation barrier require a relatively high reaction temperature for the heterolytic dissociation of H<sub>2</sub> on CeO<sub>2</sub>(111). As shown in Table S3 and Figure S1, we can see H binding strength increases with the Ce-H bond length increasing from 2.2 to 2.5 Å where a chemical bond can be formed between Ce and H. However, H binding energy becomes +2.2 eV when the bond distance between H and Ce is larger than 2.6 Å indicating the physisorption of the H atom at the Ce cation site. As a result, the formed H anion at the Ce cation is ready to migrate to the neighboring O atom with a low activation barrier of 0.14 eV on the CeO<sub>2</sub>(111) surface. Therefore, only H<sup>+</sup> can be found once H<sub>2</sub> dissociates on the CeO<sub>2</sub>(111) surface.

Heterolytic dissociation of H<sub>2</sub> is more feasible on CeO<sub>2</sub>(110) as compared with that on CeO<sub>2</sub>(111) surface (Figure 3). The calculated reaction energy and activation barrier for the heterolytic dissociation of H<sub>2</sub> is moderate over the CeO<sub>2</sub>(110) surface with the values of 0.37 eV and 0.59 eV, respectively. The activation barriers for the recombination of H<sup>-</sup> and H<sup>+</sup> in the formation of H<sub>2</sub> and the migration of H<sup>-</sup> from the Ce cation to the O anion are comparable over CeO<sub>2</sub>(110) surface with the values of 0.22 and 0.15 eV, respectively. Therefore, one can observe abundant H<sup>+</sup> on the CeO<sub>2</sub>(110) surface with rare H<sup>-</sup> anions adsorption at the Ce cation site. Especially on the CeO<sub>2</sub>(110) surface, some O anions can coordinate with two Ce<sup>3+</sup>. The Bader charge of this kind of the O anion is high that fewer electrons can be exchanged with H. That's why the charge of the H ions binding with the O anion is zero or even negative (Table S2).

The heterolytic dissociation of H<sub>2</sub> is most feasible on the CeO<sub>2</sub>(100) surface with the lowest activation barrier of 0.43 eV among the three considered CeO<sub>2</sub> surfaces due to the highly exothermic nature of the H<sub>2</sub> dissociation over the CeO<sub>2</sub>(100) surface ( $\Delta H = -0.22$  eV). After, H anion adsorbed at the Ce cation site can diffuse to the O anion site exothermically with a low activation barrier of 0.32 eV. Therefore, only H<sup>+</sup> can be found on the CeO<sub>2</sub>(100) surface which has similar catalytic behavior but more active than the CeO<sub>2</sub>(111) surface at relatively high temperatures. Our DFT calculations clearly revealed the difficulty of H<sub>2</sub> activation on the CeO<sub>2</sub>(111) surface but much feasible on the open CeO<sub>2</sub>(110) and (100) surfaces. Our result



is in line with other theoretical and experimental works that the H<sub>2</sub> dissociation is difficult on the stoichiometric CeO<sub>2</sub>(111) surface<sup>[20,22,40,50]</sup>. A large number of stable hydroxyl groups can be generated on the three different stoichiometric CeO<sub>2</sub> surfaces for the H<sub>2</sub> activation. Therefore, a high reaction temperature is required for the hydrogenation of alkynes by the usage of H cation as the hydrogen resources. The hydrogen-to-acetylene ratio is usually larger than 20 that a large number of H<sub>2</sub> molecules can be activated providing enough H<sup>+</sup> species used for acetylene hydrogenation reactions<sup>[19,20]</sup>.

### 3.2 Structure sensitivity of H<sub>2</sub> activation over defective CeO<sub>2</sub> surfaces

Oxygen vacancies often present on the CeO<sub>2</sub> surface inevitably under the acetylene hydrogenation reaction conditions. We studied the heterolytic H<sub>2</sub> dissociation mechanism over defective CeO<sub>2</sub> (111), (110), and (100) surfaces to reveal the oxygen vacancy effect on H<sub>2</sub> dissociation activity and corresponding surface H<sup>+</sup>/H<sup>-</sup> species distributions. The oxygen vacancy concentrations are different over (111), (110), and (100) surfaces with the values of 25% and 12.5%, 11.1%, respectively. The corresponding concentrations of Ce<sup>3+</sup> over the three surfaces are around 12.5% to 8.3%, which are similar to the reduced CeO<sub>2</sub> materials prepared in experiments<sup>[36,51-53]</sup> with the Ce<sup>3+</sup> concentration of 10% to 15%. The calculated optimal potential energy diagram for heterolytic H<sub>2</sub> dissociation and corresponding transition state configurations over the three defective CeO<sub>2</sub> surfaces are shown in Figure 4. The configurations of heterolytic dissociative of H<sub>2</sub> and corresponding structural information are shown in Figure S2 and Table S4, respectively. Similar to stoichiometric CeO<sub>2</sub> surfaces, H<sub>2</sub> still adsorbs weakly on the three considered defective CeO<sub>2</sub> surfaces with the adsorption energies of ~ -0.10 eV. However, the heterolytic H<sub>2</sub> dissociation is accelerated by the introduction of oxygen vacancies in CeO<sub>2</sub> surfaces from both thermodynamic and kinetic aspects (Figure 4). From the thermodynamic data in Table S4, we can see that on the defective CeO<sub>2-x</sub>(111), (110), and (100) surfaces, H<sup>-</sup> prefers to adsorb at the oxygen vacancy site, whereas H<sup>+</sup> prefer to bound with the surface oxygen atoms rather than subsurface oxygen atoms (Figure S2). For the defective CeO<sub>2-x</sub>(111) surface, the heterolytic H<sub>2</sub> dissociative adsorption energy is -0.92 eV, which is much lower than that on the stoichiometric CeO<sub>2</sub>(111) surface by 1.73 eV. As compared with stoichiometric CeO<sub>2</sub>(110) and (100) surfaces, the defective surfaces have lower heterolytic H<sub>2</sub> dissociative adsorption energies of -0.67 eV and -0.68 eV, which are lower than those on the stoichiometric surfaces by 0.98 eV and

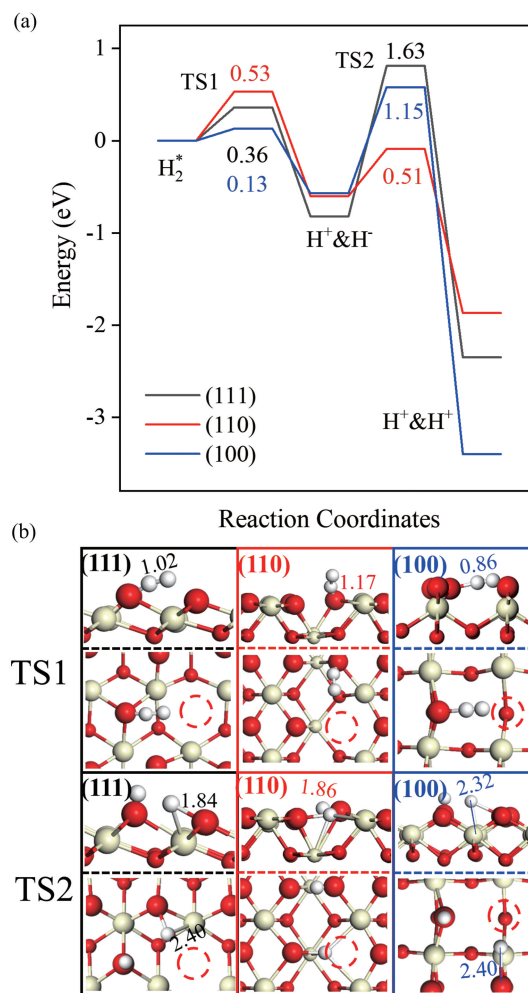


**Figure 4.** Potential energy surface diagram (a) and corresponding transition state configurations (b) for the heterolytic H<sub>2</sub> dissociation over the defective CeO<sub>2</sub> (111), (110), and (100) surfaces. The bond distances between the two dissociated H atoms are indicated in Å. Dashed red circles representing oxygen vacancies.

0.34 eV, respectively. Heterolytic H<sub>2</sub> dissociation is structure sensitive and the presence of oxygen vacancy can enhance the heterolytic H<sub>2</sub> dissociation thermodynamically.

The activation barrier of heterolytic H<sub>2</sub> dissociation forming H<sup>+</sup> and H<sup>-</sup> species is reduced by the introduction of oxygen vacancy in CeO<sub>2</sub>(111), (110), and (100) surfaces by 0.79, 0.23, and 0.30 eV, respectively. Therefore, the heterolytic H<sub>2</sub> dissociation can be accelerated on the defective CeO<sub>2</sub> surfaces as compared with the stoichiometric ones. However, H<sup>-</sup> adsorption at the Ce cation site migrates to the O anion nearby has higher or comparable reaction barriers on the defective CeO<sub>2</sub>(111), (110), and (100) surfaces as compared with those on the perfective ones by 1.49, -0.01, and 0.83 eV, respectively. This can be attributed to the less exothermic nature of the

hydrogenation migration with the introduction of oxygen vacancy in stoichiometric  $\text{CeO}_2$  surfaces.

Different from the observations of merely  $\text{H}^+$  on the three stoichiometric  $\text{CeO}_2$  surfaces,  $\text{H}^+$  and  $\text{H}^-$  can be found at a low temperature on the partially reduced  $\text{CeO}_{2-x}$ (111) and  $\text{CeO}_{2-x}$ (100) surfaces due to the higher activation barriers for  $\text{H}^-$  at the Ce cation site migration to O anion site forming  $\text{H}^+$  species of 1.63 and 1.15 eV, respectively. The heterolytic  $\text{H}_2$  dissociation and  $\text{H}^-$  migration from Ce to O forming  $\text{H}^+$  have similar activation barriers of 0.53 and 0.51 eV over  $\text{CeO}_{2-x}$ (110) surface, respectively. However, the potential energy surface goes down for  $\text{H}_2$  dissociation forming two  $\text{H}^+$  species with low activation barriers that only  $\text{H}^+$  species can be found on the defective  $\text{CeO}_2$ (110) surface. The different catalytic behaviors of the  $\text{H}_2$  dissociation between (110) and (111)/(100) surfaces can be attributed to the different bond strength of  $\text{H}^+/\text{H}^-$  on defective  $\text{CeO}_2$  surfaces.

As stated above, the heterolytic  $\text{H}_2$  dissociation is sensitive to the surface structures of  $\text{CeO}_2$  and oxygen vacancy plays an important role in the heterolytic dissociation of  $\text{H}_2$  and migration of H atom from the Ce cation site to the O anion site. This can be originated from different oxygen vacancy formation energies over different stoichiometric  $\text{CeO}_2$  surfaces. The defective  $\text{CeO}_2$  surfaces have higher activities for the heterolytic  $\text{H}_2$  dissociation than H species migration from the Ce cation to the O anion except for the perfect and defective  $\text{CeO}_2$ (110) surface sharing almost the same activities on the H migration. As a result, the surface stably adsorbed H species vary greatly over different stoichiometric and defective  $\text{CeO}_2$  surfaces that only  $\text{H}^+$  can be found on perfect  $\text{CeO}_2$  surfaces and defective  $\text{CeO}_2$ (110) surface but both  $\text{H}^+$  and  $\text{H}^-$  can be observed on the defective (111) and (100) surfaces. The different forms of H species might display distinct catalytic behaviors for acetylene hydrogenation reactions.

To further reveal the reason for the surface sensitivity of the  $\text{H}_2$  dissociation, we calculated the binding energies of  $\text{H}^+$  and  $\text{H}^-$  on stoichiometric and defective  $\text{CeO}_2$  surfaces. In Figure S3, the sum of the isolated adsorption energies of  $\text{H}^+$  and  $\text{H}^-$  is close to the coadsorption energy of the  $\text{H}^+ & \text{H}^-$  configuration. Therefore, there is no obvious interaction between the two  $\text{H}^+$  and  $\text{H}^-$  ions due to the long distance between them for the coadsorption of  $\text{H}^+ & \text{H}^-$  species. By carefully evaluating the calculated  $\text{H}^+ & \text{H}^-$  binding energies and oxygen vacancy formation energies, we find a linear scaling relationships between  $\text{H}^+/\text{H}^-$  binding energies and oxygen vacancy formation energies

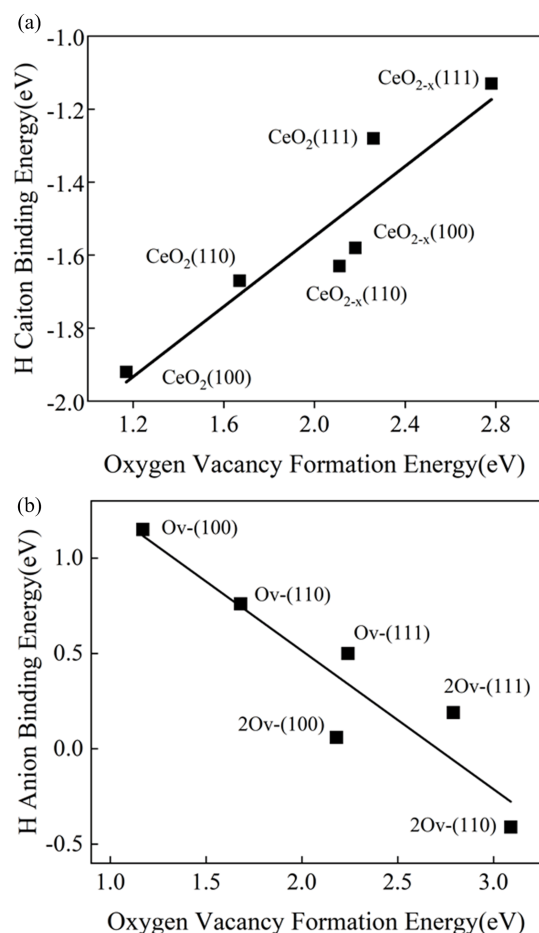


**Figure 5.** The linear scaling relationship between  $\text{H}^+$  (a)/ $\text{H}^-$  (b) binding energy and oxygen vacancy formation energy on the three reduced  $\text{CeO}_{2-x}$  surfaces.

(Figure 5). Generally, the binding strength of  $\text{H}^+$  bounded to the O anion decreases by increasing the oxygen vacancy formation energy. The calculated oxygen vacancy formation energies on (111), (110), and (100) are 2.26, 1.67, and 1.17 eV, and the corresponding Bader charge state of O over the three surfaces are  $-1.09$ ,  $-0.98$ , and  $-0.92$ , respectively. The stronger interaction between Ce and O will result in a larger Bader charge state of O cation weakening  $\text{H}^+$  adsorption. The same observations can be found on the defective  $\text{CeO}_2$  surfaces (Table S5). The surface sensitivity of homolytic adsorption is strongly correlated with the binding energy of  $\text{H}^+$ , which is determined by the ability of oxygen vacancy formation dependent on the  $\text{CeO}_2$  surfaces. We further calculated hydrogen adsorption over the reduced  $\text{CeO}_{2-x}$  surfaces with two oxygen vacancies with the concentration of  $\text{Ce}^{3+}$  of 25% to 16.6%. The relationship established between the H adsorption energy and the oxygen vacancy formation energy is still valid and universal even considering high  $\text{Ce}^{3+}$  concentrations in the slab models (Figure S4).

H<sup>-</sup> adsorption strength has an opposite trend as a function of the oxygen vacancy formation energies (Figure 5(b)). Generally, the harder the surface is to be reduced, the stronger bond can be formed between the Ce cation and the H anion. Compared with perfect surfaces, the Bader charge states of Ce cations over the defective CeO<sub>2</sub>(111), (110), and (100) surfaces are also reduced to +1.01, +1.91, +2.15, respectively. The weaker charge state of Ce adsorbs H<sup>-</sup> stronger at the Ce cation site due to the formation of the stronger covalent bond between H and Ce. This finding can be observed over the defective CeO<sub>2</sub> surfaces with two oxygen vacancies. As shown in Figure S5, it is found that there is no obvious relationship between the hydrogen activation barrier and oxygen vacancy formation energy. Due to the oxygen vacancies on the defective CeO<sub>2</sub> surface, the energy barrier for hydrogen dissociation is significantly reduced, and the surface is also more difficult to be further reduced. If the data is not classified, it does not comply with the law that the higher the oxygen vacancy formation energy, the higher the dissociation energy barrier. If discussed separately, it can be seen that the activation barriers for hydrogen activation are closely related to oxygen vacancy formation energy, that is, the higher oxygen vacancy formation energy, the higher hydrogen activation barrier on the stoichiometric and defective CeO<sub>2</sub> surfaces.

## 4 Conclusions

In the present work, we studied H<sub>2</sub> activation over the stoichiometric and defective CeO<sub>2</sub>(111), (110), and (100) surfaces. The heterolytic H<sub>2</sub> dissociation pathway is dominant on stoichiometric and defective CeO<sub>2</sub> surfaces. We identified that the heterolytic H<sub>2</sub> dissociation is difficult on the stoichiometric CeO<sub>2</sub>(111) surface corroborated by previous experimental measurements. CeO<sub>2</sub>(100) and (110) surfaces are more active than (111) surfaces for the heterolytic H<sub>2</sub> dissociation. Only the H<sup>+</sup> adsorption at the O anions can be found on all three stoichiometric CeO<sub>2</sub> surfaces. The presence of oxygen vacancies can promote the heterolytic H<sub>2</sub> dissociation over defective CeO<sub>2</sub> surfaces. Both H<sup>+</sup> and H<sup>-</sup> can be found on the defective CeO<sub>2</sub>(111) and (100) surfaces, whereas only H<sup>+</sup> species can be found on the CeO<sub>2</sub>(110) surface. The oxygen vacancy formation energy can be considered as a key descriptor for the activity of the heterolytic H<sub>2</sub> dissociation and the distribution of H<sup>+</sup>/H<sup>-</sup> species. Our work provides more insight into H<sub>2</sub> activation on CeO<sub>2</sub>-based catalysts, which is pivotal for better catalyst design.

## Supplementary data

Supplementary data are available at J. Univ. Sci. Tech. China online.

## Acknowledgments

This work was supported by the Key Technologies R&D Program of China (2017YFB0602205, 2018YFA0208603), the National Natural Science Foundation of China (91945302), the Chinese Academy of Sciences Key Project (QYZDJ-SSW-SLH054), the start-up funds of University of Science and Technology of China (KY2060000171), USTC Research Funds of the Double First-Class Initiative (YD2060002012) and high-performance computational resources provided by University of Science and Technology of China (<http://scc.ustc.edu.cn>).

## Conflict of interest

The authors declare no conflict of interest.

## Author information

**Chen Zihui** is currently a graduate student in the Department of Chemical Physics, School of Chemistry and Materials Science under the supervision of Prof. Li Weixue at University of Science and Technology of China. Her research mainly focuses on hydrogen activation on oxides surfaces.

**Liu Jinxun** (corresponding author) is currently working as a research fellow at the School of Chemistry and Materials Science, University of Science and Technology of China. He received his PhD degree from Dalian Institute of Chemical Physics and was a postdoctoral fellow in the Department of Chemical Engineering and Chemistry, Eindhoven University of Technology and in the Department of Chemical Engineering, University of Michigan-Ann Arbor. His research expertise spans computational heterogeneous catalysis, electrocatalysis, machine learning, and molecular simulation.

**Li Weixue** (corresponding author) received his PhD degree from the Chinese Academy of Sciences in 1998. He did his postdoctoral research at Fritz Haber Institut der MPG and University of Aarhus from 1999 to 2004. He joined the Dalian Institute of Chemical Physics and led the "Theoretical Catalysis Group" at the State Key Laboratory of Catalysis from 2004 to 2015. Since 2015, he is the Professor of Chemistry at University of Science and Technology of China. His research focuses on the computational and AI investigation of heterogeneous catalysis, particularly on the hydrocarbon conversion and design of the ultrastable nanocatalysts.

## References

- [1] Riley C, Zhou S, Kunwar D, et al. Design of effective catalysts for selective alkyne hydrogenation by doping of ceria with a single-atom promotor. *Journal of the American Chemical Society*, 2018, 140 (40): 12964–12973.
- [2] Teschner D, Borsodi J, Woosch A, et al. The roles of subsurface carbon and hydrogen in palladium-catalyzed alkyne hydrogenation. *Science*, 2008, 320 (5872): 86–89.

- [ 3 ] Studt F, Abild-Pedersen F, Bligaard T, et al. Identification of non-precious metal alloy catalysts for selective hydrogenation of acetylene. *Science*, 2008, 320 ( 5881 ): 1320.
- [ 4 ] Khan N A, Shaikhutdinov S, Freund H J. Acetylene and ethylene hydrogenation on alumina supported Pd-Ag model catalysts. *Catalysis Letters*, 2006, 108 ( 3 ): 159–164.
- [ 5 ] Hannagan R T, Giannakakis G, Flytzani-Stephanopoulos M, et al. Single-atom alloy catalysis. *Chemical Reviews*, 2020, 120 ( 21 ): 12044–12088.
- [ 6 ] Huang F, Deng Y, Chen Y, et al. Atomically dispersed Pd on nanodiamond/graphene hybrid for selective hydrogenation of acetylene. *Journal of the American Chemical Society*, 2018, 140 ( 41 ): 13142–13146.
- [ 7 ] Zhuo H Y, Yu X, Yu Q, et al. Selective hydrogenation of acetylene on graphene-supported non-noble metal single-atom catalysts. *Science China Materials*, 2020, 63 ( 9 ): 1741–1749.
- [ 8 ] Vanni M, Serrano-Ruiz M, Telesio F, et al. Black phosphorus/palladium nanohybrid: Unraveling the nature of P-Pd interaction and application in selective hydrogenation. *Chemistry of Materials*, 2019, 31 ( 14 ): 5075–5080.
- [ 9 ] Farnesi Camellone M, Negreiros Ribeiro F, Szabová L, et al. Catalytic proton dynamics at the water/solid interface of ceria-supported Pt clusters. *Journal of the American Chemical Society*, 2016, 138 ( 36 ): 11560–11567.
- [ 10 ] Ye X, Wang H, Lin Y, et al. Insight of the stability and activity of platinum single atoms on ceria. *Nano Research*, 2019, 12 ( 6 ): 1401–1409.
- [ 11 ] ParastaeV A, Muravev V, Osta E, et al. Boosting CO<sub>2</sub> hydrogenation via size-dependent metal-support interactions in cobalt/ceria-based catalysts. *Nature Catalysis*, 2020, 3: 526–533.
- [ 12 ] Kašpar J, Fornasiero P, Graziani M. Use of CeO<sub>2</sub>-based oxides in the three-way catalysis. *Catalysis Today*, 1999, 50 ( 2 ): 285–298.
- [ 13 ] Eguchi K, Setoguchi T, Inoue T, et al. Electrical properties of ceria-based oxides and their application to solid oxide fuel cells. *Solid State Ionics*, 1992, 52 ( 1 ): 165–172.
- [ 14 ] Liu Z, Ding D, Liu M, et al. High-performance, ceria-based solid oxide fuel cells fabricated at low temperatures. *Journal of Power Sources*, 2013, 241: 454–459.
- [ 15 ] Rajabbeigi N, Elyassi B, Khodadadi A, et al. A novel miniaturized oxygen sensor with solid-state ceria-zirconia reference. *Sensors and Actuators B: Chemical*, 2004, 100 ( 1 ): 139–142.
- [ 16 ] Izu N, Shin W, Matsubara I, et al. Development of resistive oxygen sensors based on cerium oxide thick film. *Journal of Electroceramics*, 2004, 13 ( 1 ): 703–706.
- [ 17 ] Montini T, Melchionna M, Monai M, et al. Fundamentals and catalytic applications of CeO<sub>2</sub>-based materials. *Chemical Reviews*, 2016, 116 ( 10 ): 5987–6041.
- [ 18 ] Paier J, Penschke C, Sauer J. Oxygen defects and surface chemistry of ceria: Quantum chemical studies compared to experiment. *Chemical Reviews*, 2013, 113 ( 6 ): 3949–3985.
- [ 19 ] Vilé G, Bridier B, Wichert J, et al. Ceria in hydrogenation catalysis: High selectivity in the conversion of alkynes to olefins. *Angewandte Chemie International Edition*, 2012, 51 ( 34 ): 8620–8623.
- [ 20 ] Carrasco J, Vilé G, Fernández-Torre D, et al. Molecular-level understanding of CeO<sub>2</sub> as a catalyst for partial alkyne hydrogenation. *The Journal of Physical Chemistry C*, 2014, 118 ( 10 ): 5352–5360.
- [ 21 ] Vilé G, Colussi S, Krumeich F, et al. Opposite face sensitivity of CeO<sub>2</sub> in hydrogenation and oxidation catalysis. *Angewandte Chemie International Edition*, 2014, 53 ( 45 ): 12069–12072.
- [ 22 ] Capdevila-Cortada M, García-Melchor M, López N. Unraveling the structure sensitivity in methanol conversion on CeO<sub>2</sub>: A DFT+U study. *Journal of Catalysis*, 2015, 327: 58–64.
- [ 23 ] Mullins D R. The surface chemistry of cerium oxide. *Surface Science Reports*, 2015, 70 ( 1 ): 42–85.
- [ 24 ] García-Mota M, Gómez-Díaz J, Novell-Leruth G, et al. A density functional theory study of the ‘mythic’ Lindlar hydrogenation catalyst. *Theoretical Chemistry Accounts*, 2011, 128 ( 4 ): 663–673.
- [ 25 ] Vilé G, Dähler P, Vecchietti J, et al. Promoted ceria catalysts for alkyne semi-hydrogenation. *Journal of Catalysis*, 2015, 324: 69–78.
- [ 26 ] Ganduglia-Pirovano M V, Popa C, Sauer J, et al. Role of ceria in oxidative dehydrogenation on supported vanadia catalysts. *Journal of the American Chemical Society*, 2010, 132 ( 7 ): 2345–2349.
- [ 27 ] da Silva Alvim R, Borges I, Leitão A A. Proton migration on perfect, vacant, and doped MgO(001) surfaces: Role of dissociation residual groups. *The Journal of Physical Chemistry C*, 2018, 122 ( 38 ): 21841–21853.
- [ 28 ] Chen H Y T, Giordano L, Pacchioni G. From heterolytic to homolytic H<sub>2</sub> dissociation on nanostructured MgO(001) films as a function of the metal support. *The Journal of Physical Chemistry C*, 2013, 117 ( 20 ): 10623–10629.
- [ 29 ] Martin D, Duprez D. Mobility of surface species on oxides. 1. Isotopic exchange of <sup>18</sup>O<sub>2</sub> with <sup>16</sup>O of SiO<sub>2</sub>, Al<sub>2</sub>O<sub>3</sub>, ZrO<sub>2</sub>, MgO, CeO<sub>2</sub>, and CeO<sub>2</sub>-Al<sub>2</sub>O<sub>3</sub>. Activation by noble metals. Correlation with oxide basicity. *The Journal of Physical Chemistry*, 1996, 100 ( 22 ): 9429–9438.
- [ 30 ] García-Melchor M, López N. Homolytic products from heterolytic paths in H<sub>2</sub> dissociation on metal oxides: The example of CeO<sub>2</sub>. *The Journal of Physical Chemistry C*, 2014, 118 ( 20 ): 10921–10926.
- [ 31 ] Syzgantseva O, Calatayud M, Minot C. Hydrogen adsorption on monoclinic (111) and (101) ZrO<sub>2</sub> surfaces: A periodic ab initio study. *The Journal of Physical Chemistry C*, 2010, 114 ( 27 ): 11918–11923.
- [ 32 ] Wu Z, Zhang W, Xiong F, et al. Active hydrogen species on TiO<sub>2</sub> for photocatalytic H<sub>2</sub> production. *Physical Chemistry Chemical Physics*, 2014, 16 ( 15 ): 7051–7057.
- [ 33 ] Schweke D, Shelly L, Ben David R, et al. A comprehensive study of the ceria-H<sub>2</sub> system: Effect of the reaction conditions on the reduction extent and intermediates. *The Journal of Physical Chemistry C*, 2020, 124 ( 11 ): 6180–6187.
- [ 34 ] Menetrey M, Markovits A, Minot C. Reactivity of a reduced metal oxide surface: Hydrogen, water and carbon monoxide adsorption on oxygen defective rutile TiO<sub>2</sub>(110). *Surface Science*, 2003, 524 ( 1 ): 49–62.



- [35] Huang Z Q, Liu L P, Qi S, et al. Understanding all-solid frustrated Lewis pair sites on CeO<sub>2</sub> from theoretical perspectives. *ACS Catalysis*, 2018, 8 (1): 546–554.
- [36] Li Z, Werner K, Qian K, et al. Oxidation of reduced ceria by incorporation of hydrogen. *Angewandte Chemie International Edition*, 2019, 58 (41): 14686–14693.
- [37] Wu Z, Cheng Y, Tao F, et al. Direct neutron spectroscopy observation of cerium hydride species on a cerium oxide catalyst. *Journal of the American Chemical Society*, 2017, 139 (28): 9721–9727.
- [38] Cao T, You R, Li Z, et al. Morphology-dependent CeO<sub>2</sub> catalysis in acetylene semihydrogenation reaction. *Applied Surface Science*, 2020, 501: 144120.
- [39] Vilé G, Colussi S, Krumeich F, et al. Opposite face sensitivity of CeO<sub>2</sub> in hydrogenation and oxidation catalysis. *Angewandte Chemie International Edition*, 2014, 53 (45): 12069–12072.
- [40] Matz O, Calatayud M. Breaking H<sub>2</sub> with CeO<sub>2</sub>: Effect of surface termination. *ACS Omega*, 2018, 3 (11): 16063–16073.
- [41] Kresse G, Hafner J. Ab initio molecular dynamics for liquid metals. *Physical Review B*, 1993, 47 (1): 558–561.
- [42] Kresse G, Furthmüller J. Efficient iterative schemes for ab initio total-energy calculations using a plane-wave basis set. *Physical Review B*, 1996, 54 (16): 11169–11186.
- [43] Perdew J P, Burke K, Ernzerhof M. Generalized gradient approximation made simple [Phys. Rev. Lett. 77, 3865 (1996)]. *Physical Review Letters*, 1997, 78 (7): 1396.
- [44] Kresse G, Joubert D. From ultrasoft pseudopotentials to the projector augmented-wave method. *Physical Review B*, 1999, 59: 1758.
- [45] Kümmerle E A, Heger G. The structures of C–Ce<sub>2</sub>O<sub>3+δ</sub>, Ce<sub>7</sub>O<sub>12</sub>, and Ce<sub>11</sub>O<sub>20</sub>. *Journal of Solid State Chemistry*, 1999, 147 (2): 485–500.
- [46] Castleton C W, Kullgren J, Hermansson K. Tuning LDA+U for electron localization and structure at oxygen vacancies in ceria. *The Journal of Chemical Physics*, 2007, 127 (24): 244704.
- [47] Tasker P W. The stability of ionic crystal surfaces. *Journal of Physics C: Solid State Physics*, 1979, 12 (22): 4977–4984.
- [48] Zhou C Y, Wang D, Gong X Q. A DFT+U revisit of reconstructed CeO<sub>2</sub> (100) surfaces: Structures, thermostabilities and reactivities. *Physical Chemistry Chemical Physics*, 2019, 21 (36): 19987–19994.
- [49] Kim Y, Lee H, Kwak J H. Mechanism of CO oxidation on Pd/CeO<sub>2</sub> (100): The unique surface-structure of CeO<sub>2</sub> (100) and the role of peroxide. *ChemCatChem*, 2020, 12 (20): 5164–5172.
- [50] Chen H T, Choi Y M, Liu M, et al. A theoretical study of surface reduction mechanisms of CeO<sub>2</sub> (111) and (110) by H<sub>2</sub>. *ChemPhysChem*, 2007, 8 (6): 849–855.
- [51] Li Z, Werner K, Chen L, et al. Interaction of hydrogen with ceria: Hydroxylation, reduction, and hydride formation on the surface and in the bulk. *Chemistry*, 2021, 27 (16): 5268–5276.
- [52] Özkan E, Cop P, Benfer F, et al. Rational synthesis concept for cerium oxide nanoparticles: On the impact of particle size on the oxygen storage capacity. *The Journal of Physical Chemistry C*, 2020, 124 (16): 8736–8748.
- [53] Dutta P, Pal S, Seehra M S, et al. Concentration of Ce<sup>3+</sup> and oxygen vacancies in cerium oxide nanoparticles. *Chemistry of Materials*, 2006, 18 (21): 5144–5146.

## 基于第一性原理的二氧化铈完整和缺陷表面上氢气活化研究

陈姊慧<sup>1</sup>, 赵川林<sup>1</sup>, 刘进勋<sup>1\*</sup>, 李微雪<sup>1,2\*</sup>

1. 中国科学技术大学化学与材料科学学院化学物理系, 安徽合肥 230026;

2. 中国科学技术大学合肥微尺度物质科学国家研究中心, 安徽合肥 230026

\* 通讯作者. E-mail: jxliu86@ustc.edu.cn; wxli70@ustc.edu.cn

**摘要:** 氢气活化在过渡金属氧化物催化的加氢反应中起到至关重要的作用。二氧化铈(CeO<sub>2</sub>)表面上氢气如何活化是乙炔加氢反应中的重要科学问题。本文利用密度泛函理论计算(DFT)的方法,系统研究了化学计量及有氧缺陷的CeO<sub>2</sub>(111)、(110)和(100)表面上氢气活化机理。氢气在化学计量的CeO<sub>2</sub>表面解离时仅形成羟基,而氧空位的存在可以有效促进氢气活化。CeO<sub>2-x</sub>(111)和(100)缺陷表面上H<sup>+</sup>和H<sup>-</sup>物种可以共存,而在CeO<sub>2-x</sub>(110)缺陷表面上只能观察到H<sup>+</sup>物种。化学计量及有氧缺陷的CeO<sub>2</sub>表面上氢气活化的结构敏感性与H<sup>+</sup>和H<sup>-</sup>吸附能有关,并由氧空位形成能以及Ce、O离子的电荷分布决定。该理论工作深入理解了二氧化铈基催化剂上氢气活化过程,为优化和设计高效加氢催化剂提供了理论支撑。

**关键词:** 二氧化铈; 氢气活化; 表面敏感性; 密度泛函理论